Demonstration of a silicon-based quantum cellular automata cell

M. Mitic,[a] M. C. Cassidy, K. D. Petersson,[b] R. P. Starrett, E. Gauja, R. Brenner,
R. G. Clark, and A. S. Dzurak
*Centre for Quantum Computer Technology, School of Electrical Engineering and School of Physics, The
University of New South Wales, Sydney, New South Wales 2052, Australia*

C. Yang and D. N. Jamieson
*Centre for Quantum Computer Technology, School of Physics, University of Melbourne, Victoria 3010,
Australia*

We report on the demonstration of a silicon-based quantum cellular automata (QCA) unit cell incorporating two pairs of metallically doped (n^+) phosphorus-implanted nanoscale dots, separated from source and drain reservoirs by nominally undoped tunnel barriers. Metallic cell control gates, together with Al–AlO$_x$ single electron transistors for noninvasive cell-state readout, are located on the device surface and capacitively coupled to the buried QCA cell. Operation at subkelvin temperatures was demonstrated by switching of a single electron between output dots, induced by a driven single electron transfer in the input dots. The stability limits of the QCA cell operation were also determined. © *2006 American Institute of Physics.* [DOI: 10.1063/1.2219128]

Quantum cellular automata[1] (QCA) is a computation paradigm based on single electron charge control, providing potential solutions to the critical problems of device density, interconnection, and power dissipation. The basic cell of a QCA comprises four quantum or metallic dots coupled by tunnel barriers [Fig. 1(a)]. If two electrons are added to the cell, their mutual electrostatic repulsion forces them to occupy diagonal sites, giving rise to two possible cell polarization states. These states can be used to encode and process binary information.[1]

To date, QCA cells have been experimentally demonstrated using Al metallic dots[2] and magnetic dot systems,[3] with promising results also in using GaAs quantum dots.[4] Here we report the experimental demonstration of a QCA unit cell in an ion-implanted phosphorus-doped silicon (Si:P) system. Si:P QCA offer advantages including compatibility with scalable Si microfabrication technologies and scope for cell size reduction down to the single donor level, offering the possibility of fast (subnanosecond), low-power charge-based computing with bit cell sizes below 50 nm.[5]

The circuit equivalent of our QCA cell is shown in Fig. 1, together with scanning electron microscopy (SEM) images of the device. Four implanted (n^+) Si:P dots are arranged in tunnel-coupled pairs (*A* and *B*), each tunnel coupled to an electron reservoir. The two dot pairs are capacitively coupled to each other, but separated by a distance sufficient to prevent electron transfer *between* pairs. The source and drain reservoirs allow characterization of the cell via direct current measurement and also enable the total electron occupancy of the cell to be adjusted. In multicell systems these reservoirs may be omitted to maximize packing density. Control of electron number occupancy $\{n_A, m_A, n_B, m_B\}$ within the cell is provided by four surface gates, while two Al–AlO$_x$ single electron transistors (SETs) on the surface provide *noninvasive* charge-state readout,[6] as previously demonstrated in Si:P double dots.[7]

The devices were fabricated from near-intrinsic ($n < 10^{12}$ cm^{-3}) silicon with resistivity above 5 kΩ cm, terminated by a 5 nm thick layer of thermally grown SiO$_2$. To form the QCA cell, four n^+ islands (500 nm × 80 nm) with leads were defined by phosphorus ion implantation through a polymethyl-methacrylate (PMMA) resist mask patterned by electron beam lithography (EBL). A rapid thermal annealing at 1000 °C for 5 s was performed to repair implant damage and activate the donors. The 14 keV ^{31}P$^+$ beam produced a mean implantation depth $\sim$15 nm below the Si–SiO$_2$ interface and a doping density $n^+ \sim 10^{19}$ cm^{-3}, an order of magnitude above the metal-insulator transition. The near-intrinsic Si substrate acts as a tunnel barrier between n^+ regions at low temperature. To allow tunneling between adjacent dots and reservoirs (within half-cells *A* and *B*) we set a tunnel barrier width $\sim$60 nm, while a separation between the half-cells of $\sim$220 nm was sufficient to suppress tunneling [see SEM of implanted regions in Fig. 1(b)]. At 50 mK the source-drain resistance for each half-cell was measured to be $\sim$5
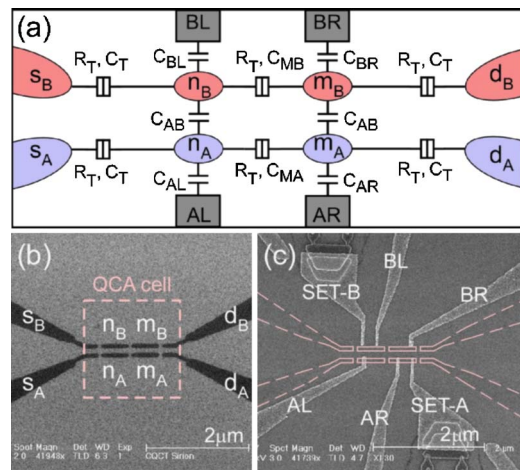

FIG. 1. (Color online) (a) Simplified circuit equivalent of the QCA cell, (b) SEM image of phosphorus-implanted n^+ regions (dark in image), and (c) SEM image of completed device. The buried n^+ dots and leads are marked using dashed lines.

[a] Electronic mail: m.mitic@student.unsw.edu.au
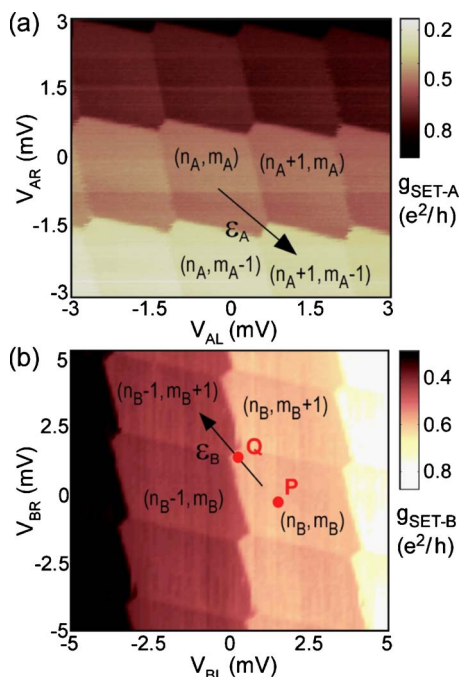[b] Currently at Cavendish Laboratory, University of Cambridge.

FIG. 2. (Color online) SET conductance intensity plots as functions of respective half-cell control gate voltages. A plane is subtracted from the raw data to remove direct gate-SET coupling. Effective gate polarizations are shown in the plots as ε_A and ε_B. (a) SET-*A* conductance showing electron occupancy (n_A, m_A) within half-cell *A*. (b) SET-*B* conductance, with half-cell *B* occupancies labeled similarly.

FIG. 3. (Color online) Normalized charge (q/e) induced on the two SETs as a function of gate polarization ε_A. Direct gate-SET coupling was subtracted from the raw data. (a) Half-cell *B* is biased at point *P*. QCA operation is not observed; (b) half-cell *B* is biased at point *Q*. As ε_A is swept, SET-*A* detects electron tunneling in half-cell *A*, which induces a transition in half-cell *B* (see inset). QCA operation is therefore realized.

$\times 10^7$ Ω, while the resistance between half-cells (i.e., between s_A and s_B) was $>10^{12}$ Ω, consistent with the QCA cell design requirements.

Nanocircuitry for control and readout was fabricated on the device surface, insulated from the implanted Si:P dots by the SiO$_2$ layer. Standard EBL patterning of PMMA and lift-off were used to define Ti/Au control gates, together with electrodes that extend the SET islands above the buried Si:P dots to maximize capacitive coupling [see Fig. 1(c)]. The two Al−AlO$_x$ readout SETs were fabricated last, using EBL patterning of a bilayer resist and double-angle evaporation of aluminum.[8]

Electrical measurements were performed in a dilution refrigerator operated at a base temperature below 50 mK, with an applied magnetic field of 0.5 T used to suppress superconductivity in the aluminum. The SETs were operated as sensitive charge detectors[6] by applying compensating voltages to their bias gates whenever the QCA control gate voltages were varied. Throughout the QCA demonstration measurements both SETs were biased on the *descending* sides of their Coulomb oscillation peaks, in order to distinguish the direction of electron transfers detected.[9] The source and drain leads of both double dots were grounded.

Prior to operation of the QCA cell, it was necessary to map the charge state $\{n_i, m_i\}$ of each double-dot half-cell as a function of its two control gate voltages, where n_i (m_i) refers to the electron occupancy number of the left (right) dot of half-cell i. Figure 2(a) and 2(b) plots the normalized conductance of SET-*A* (SET-*B*) as a function of the control gate voltages on half-cell *A* (*B*). We observe that SET-*A* is more sensitive to changes in m_A than changes in n_A, while SET-*B* senses changes in n_B better than m_B. This is expected from the device geometry [see Fig. 1(c)], as the island of SET-*A* (SET-*B*) is positioned above the right (left) dot. The typical
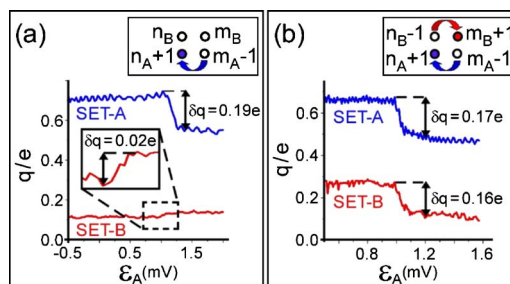
SET resistance was ~200 kΩ, while the typical charges induced on the SET islands by an electron transfer between dots in their respective half-cells were measured to be $0.23e$ for SET-*A* and $0.18e$ for SET-*B*. The difference results from cell asymmetry due to ~30 nm misalignment between the surface metallization and buried Si:P dots that led to increased capacitive coupling of SET-*A* to half-cell *A*.

From the sizes of the state cells in Fig. 2 and nonlinear transport measurements, the capacitances between the gates and their respective dots were calculated[10] to be $C_{AL}=98$ aF, $C_{AR}=75$ aF, $C_{BL}=45$ aF, and $C_{BR}=56$ aF, while the capacitances between the implanted dots were $C_{MA}=27$ aF and $C_{MB}=21$ aF. All of these values were within 20% of FASTCAP modeling predictions after correction for the misalignment discussed above. The typical charging energy of the dots, calculated from the measured capacitances, was ~0.5 meV, consistent with the modeling and with source-drain bias spectroscopy measurements on this device.

To demonstrate QCA operation we apply a differential bias between control gates *AL* and *AR*, sufficient to drive a single electron transfer within half-cell *A*. Provided the cell is biased appropriately, this leads to simultaneous electron transfer within half-cell *B*, as depicted in Fig. 3(b) (inset). The mutual repulsion of the two excess electrons leads to the state change in the cell. The differential gate bias (or polarization) can be defined as $\varepsilon_A = \cos(\theta)\, V_{AL} - \sin(\theta) V_{AR}$ for half-cell *A* and $\varepsilon_B = \cos(\phi)V_{BR} - \sin(\phi)V_{BL}$ for half-cell *B*, where θ, $\phi \sim \pi/4$.

Figure 3 plots the simultaneously measured output of both SETs as the gate polarization ε_A of half-cell *A* is varied, for two different biasing conditions of half-cell *B*. In Fig. 3(a) we bias half-cell *B* at point *P*, as shown on the stability diagram in Fig. 2(b). At $\varepsilon_A \sim 1.0$ mV the gate polarization drives an electron from the right dot to the left, in half-cell *A*. This electron transfer is detected strongly by SET-*A*, with a characteristic induced charge signal of $-0.19e$. In contrast, SET-*B* detects a much smaller signal ($+0.02e$) since it is only weakly coupled to the remote half-cell *A*. The positive sign is consistent with an electron moving *towards* the island of SET-*B*, as expected. At this particular biasing point (*P*) the electron transfer in half-cell *A* does not induce a transfer in half-cell *B* and the device does *not* operate as a QCA cell.

For QCA operation we must bias half-cell *B* near a transition point, such as point *Q* in Fig. 2(b). Figure 3(b) plots the corresponding SET outputs as we drive an electron transfer in half-cell *A*. Once again, SET-*A* detects the local trans-
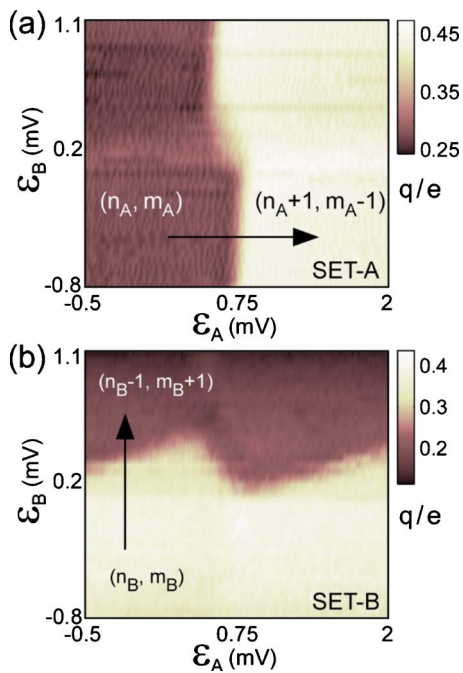
FIG. 4. (Color online) Normalized charge (q/e) induced on (a) SET-*A* and (b) SET-*B* as a function of gate polarizations ε_A and ε_B. A plane is subtracted from the raw data to remove the direct gate-SET coupling. For explanation see text.

fer with a strong signal of $-0.17e$; however, *now* SET-*B* also detects a *strong transfer* with signal $-0.16e$. This size signal can only result from a transfer *within* half-cell *B*, and the negative sign of the signal is consistent with an electron moving *away from* SET-*B*. The required QCA cell response, as depicted in the inset of Fig. 3(b), is therefore realized. From our measurements we find an induced polarization on half-cell *B* of approximately 65% due to thermal smearing. This value is design specific and is similar to the ones obtained in nonclocked aluminum QCA systems.[11]

To determine the range of bias conditions necessary for stable QCA cell operation, we repeatedly drove a charge transfer in half-cell *A* by sweeping ε_A while changing the effective polarization ε_B of half-cell *B* along the arrow shown in Fig. 2(b), following the method used in aluminum QCA systems.[12] Figure 4 plots the simultaneously measured induced charges on the two SETs as functions of the two polarizations. The strong induced charge transitions observed correspond to electron transfers within the strongly coupled half-cells. If there was no capacitive coupling between the half-cells, the loci of these transitions would be straight lines, being simple linear combinations of ε_A and ε_B. The "kinks" observed result from charge rearrangements within the opposite half-cells. More specifically, SET-*A* detects the transfer in half-cell *A*, which happens at different values of ε_A depending on the state of half-cell *B*, and vice versa. From Fig. 4 we are able to calculate the capacitance between half-cells to be $C_{AB} = \sim 30$ aF, which is consistent with our modeling. For this device we find that stable QCA operation is possible over the range of $\varepsilon_B = 0.16 - 0.64$ mV when driven by half-cell *A*, or over the range of $\varepsilon_A = 0.56 - 0.81$ mV when driven by half-cell *B*. The difference in range for the two half-cells

results from the small misalignment discussed earlier. The stability range is design specific and is critically influenced by the coupling capacitances and cross capacitances within the cell.

In summary, we have presented measurements of a four dot QCA logic cell in a phosphorus-doped silicon system. The QCA operation was demonstrated *directly*, inducing an electron transfer in one half-cell by driving the other through a transition, and *indirectly* by plotting the state space of the cell in terms of the effective gate polarizations. Given the convenient fabrication and charge stability of this Si:P cell, we expect it to be relatively straightforward to extend this architecture to more complex QCA logic such as shift registers.[13] All-silicon SETs[14] could also be incorporated for state readout, providing greater compatibility with complementary metal-oxide semiconductor (CMOS) processing. We see no reason why downscaling to QCA cells based on single dopant atoms[5] could not be achieved, using recently developed technologies such as controlled single ion implantation[15] or scanning tunneling microscopy (STM) lithography.[16] The greater electron confinement provided by single donor potentials offers the possibility of higher temperature operation, together with an ability to create fast, ultrahigh-density QCA logic devices with very low-power consumption.

[1]C. S. Lent, P. D. Tougaw, W. Porod, and G. H. Bernstein, Nanotechnology **4**, 49 (1993).
[2]A. O. Orlov, I. Amlani, G. H. Bernstein, C. S. Lent, and G. L. Snider, Science **277**, 928 (1997).
[3]R. P. Cowburn and M. E. Welland, Science **287**, 1466 (2000).
[4]S. Gardelis, C. G. Smith, J. Cooper, D. A. Ritchie, E. H. Linfield, and Y. Jin, Phys. Rev. B **67**, 033302 (2003).
[5]J. H. Cole, A. D. Greentree, C. J. Wellard, L. C. L. Hollenberg, and S. Prawer, Phys. Rev. B **71**, 115302 (2005).
[6]M. H. Devoret and R. J. Schoelkopf, Nature (London) **406**, 1039 (2000).
[7]V. C. Chan, T. M. Buehler, A. J. Ferguson, D. R. McCamey, D. J. Reilly, A. S. Dzurak, R. G. Clark, C. Yang, and D. N. Jamieson, e-print cond-mat/0602538.
[8]T. A. Fulton and G. J. Dolan, Phys. Rev. Lett. **59**, 109 (1987).
[9]T. M. Buehler, D. J. Reilly, R. Brenner, A. R. Hamilton, A. S. Dzurak, and R. G. Clark, Appl. Phys. Lett. **82**, 577 (2003).
[10]W. G. van der Wiel, S. D. Franceschi, J. M. Elzerman, T. Fujisawa, S. Tarucha, and L. P. Kouwenhoven, Rev. Mod. Phys. **75**, 1 (2003).
[11]I. Amlani, A. O. Orlov, G. L. Snider, C. S. Lent, and G. H. Bernstein, Appl. Phys. Lett. **72**, 2179 (1998).
[12]W. Porod, C. S. Lent, G. H. Bernstein, A. O. Orlov, I. Amlani, G. L. Snider, and J. L. Merz, Int. J. Electron. **86**, 549 (1999).
[13]A. O. Orlov, R. Kummamuru, R. Ramasubramaniam, C. S. Lent, G. H. Bernstein, and G. L. Snider, Surf. Sci. **532**, 1193 (2003).
[14]A. Fujiwara, H. Inokawa, K. Yamazaki, H. Namatsu, Y. Takahashi, N. M. Zimmerman, and S. B. Martin, Appl. Phys. Lett. **88**, 053121 (2006).
[15]D. N. Jamieson, C. Yang, T. Hopf, S. M. Hearne, C. I. Pakes, S. Prawer, M. Mitic, E. Gauja, S. E. Andresen, F. E. Hudson, A. S. Dzurak, and R. G. Clark, Appl. Phys. Lett. **86**, 202101 (2005).
[16]S. R. Schofield, N. J. Curson, M. Y. Simmons, F. J. Ruess, T. Hallam, L. Oberbeck, and R. G. Clark, Phys. Rev. Lett. **91**, 136104 (2003).